

Reply to Ian Jackson's review:

Reviewer: Does the 2D analysis of the wave propagation bias the estimated intensity of scattering by ignoring scattering into and out of the plane of the calculation?

Authors' response: Few tests of 2-D vs 3-D scattering effects exist. Wu and Irving (GJI, 2017, doi: 10.1093/gji/ggx047), who compared 3-D to 2.5D numerical simulations, show an example test. Their 2.5D simulations do not remove the energy of out-of-plane scattering, but they did not find significant differences between the simulations for smoothed PKiKP coda.

At any given velocity and density perturbation, however, 3-D scattering in principle should remove more energy from the direct arriving pulse than 2-D scattering in a plane containing the source, receiver, and center of the earth. Thus the assumption of 2-D scattering at a given perturbation level will potentially overestimate the true perturbation level needed to produce that apparent attenuation. Any overestimate of the perturbation level just reinforces our conclusion that intrinsic attenuation is also needed to explain the observed apparent attenuation combined with coda levels.

Authors' changes in manuscript: We added lines addressing this comment in lines 109-111.

Reviewer: To what degree are the results of this analysis influenced by the assumption of constant Q within the absorption band, rather than the mild frequency dependence ($Q \propto f^{1/3}$) consistently revealed by laboratory studies?

Author's response: Resolving the frequency dependence of intrinsic attenuation from seismic data is a notoriously difficult problem, complicated by depth dependence, and the need to compare observations over a very broad frequency band. Using observations of free-oscillations and low frequency surface waves (0.001 to 0.005 Hz), a study by Lekic et al. (EPSL, 2009, doi:10.1016/j.epsl.2009.03.030) found a power of 0.3 frequency dependence of Q_s , diminishing to 0 as frequency increased. A body wave study by Choy and Cormier (JGR, 1986, doi: 10.1029/JB091iB07p07326) found small or no frequency dependence of attenuation in the upper and lowermost mantle but attenuation decreasing with frequency as a power of -1 above a corner frequency in the mid-mantle. The frequency band of our observations and simulations, however, is too narrow (0.01 to 0.25 Hz) to observe a difference between the effects of a power of 0 or -0.3 for the frequency dependence of attenuation ($1/Q$). Our study also did not consider the complication of depth dependent changes in the shape of the relaxation spectrum, which would require both multiple S and ScS observations over a series of ranges

Authors' changes in manuscript: We added lines addressing this comment in lines 136-140

Reviewer: How was the thermodynamic model of mantle heterogeneity derived? In particular, what range of variability of chemical composition and temperature was allowed?

Authors' response: Except for a peak in heterogeneity power associated with a post-perovskite phase change in the lowermost mantle our test “maximum plausible” heterogeneity model was derived from a study of P wave coherence beneath the USArray (Cormier et al., Commun. Comp. Phys., preprint, doi: 10.4208/cicp.OA-2018-0079) , assuming $d\ln V_s/d\ln V_p = 2$. The peaks in the heterogeneity model inferred from P wave coherence closely coincide with predictions from thermodynamic models by Stixrude and Lithgow-Bertelloni, with which we were initially surprised. These thermodynamic models considered a range of mantle compositions and mixing scenarios. Details are given in several of their papers. Models of mantle compositions included both pyrolite and depleted MORB mantle, assumed both mechanical mixing and equilibrium assemblages, and considered variations in potential temperature between 1000 to 2000 deg K. Most of the differences between the models were their predictions for 1-D averages of mantle seismic velocities. There were not large differences between models for the size and position of predicted peaks of heterogeneity power at different depths, which are most important to seismic scattering.

Authors' changes in manuscript: We added lines addressing this comment in lines 65-79.

Reviewer: What is the explanation for the conclusion that the heterogeneity from the tomographic wavespeed model is insufficient to explain the amplitude of the ScS coda? Does this potentially reflect the fact that spatial smoothing tends to mean that the amplitudes of wavespeed anomalies are underestimated?

Authors' response: The heterogeneity power in these models is too weak to explain the observed ScS coda power even when we assumed a white spectrum between the scale lengths (>200 km) they can resolve and the scale length corresponding to the smallest scale (25 km) that will produce significant scattering the frequency pass band we observed and modeled. Yes, images from global tomography underestimate wavespeed anomalies by smoothing fluctuations in travel time picks. These fluctuations are due to a combination of picking errors and the effects of unresolvable small-scale structure observed over paths limited in spatial density. Regularizing parameters in tomographic inversion damp these fluctuations. To explain multi-pathing that has been observed in body waveforms some studies have multiplied the velocity perturbations in large-scale structures imaged by tomograms by factors up to 2 to explain the observed waveform complexity (e.g., Romanowicz et al., EPSL 233, 137-153, 2005).

Authors changes in manuscript: We added lines and a reference addressing this comment in lines 200-204.

Reply to anonymous reviewer:

Reviewer: The connection of the modeling results to inferences about Earth's mantle via comparison with observational results is much weaker on account of the choice to ignore the wealth of relevant and easily accessible seismic data in modern community archives. Consequently, I am cautious about the value of the interpretations regarding the balance of scattering and intrinsic attenuation in the real rather than synthetic model mantle. The observational component of the manuscript should be substantially expanded to use global data from many sources and a large number of receivers as the available data resources have advanced greatly beyond those used in most of the references. Comparing a more statistically significant set of waveform analyses to thermodynamic modeling results would be a powerful approach for evaluating the relative influences of scattering and intrinsic attenuation. Given the quality of the modeling component I would suggest focusing on that in this manuscript and refraining from insights into actual mantle properties rather than just model implications. Or, with much more observational analysis a compelling observational component could be added to this study.

Authors response: Addressing the reviewer's comment on use of dense modern waveform data, we point out that the analysis and conclusions of our paper are supported by a heterogeneity model that was determined from many 100's of waveforms observed from deep focus earthquake in 3 regions recorded by sensors in the USArray of Earthscope. The thermodynamic models are cited simply to point out their agreement with the heterogeneity spectrum we obtained from P wave coherence together with an assumed scaling between P velocity fluctuations and S velocity and density fluctuations. We clarified the connections between our heterogeneity model and the thermodynamic models in revised lines 66 -79. See also some supporting figures uploaded in our earlier reply submitted during the discussion period.

The section discussing the analysis of attenuation inverted from 2 representative deep focus earthquakes is important for demonstrating that coda levels and waveform complexity as well as the shape of the initial pulse are also important for constraining the effects of heterogeneity. We chose events that we felt represented the span of attenuation values determined in earlier works published by Sipkin, Jordan, Revenaugh, Okal, and others. We acknowledge the reviewer's point that a much larger volume of data is available for reexamining the mantle attenuation from ScSn observations. A voluminous data sample would enable stacking to more quantitatively characterize coda shapes. Our goal in this paper, however, was to simply demonstrate some maximal bounds on the contribution of scattering by choosing some representative events with quite different levels of apparent scattering in their ScSn codas.

Authors' changes in manuscript: We clarified this in revised lines 184-191 and provide a supplementary figures showing possible data available for a more complete analysis and also provide a synthetic SH record section for a deep focus earthquake to illustrate where ScS and ScSScS are observable and well separated from other phases.

1 **The relative contributions of scattering and viscoelasticity to the** 2 **attenuation of S waves in Earth's mantle**

3 Susini deSilva¹, Vernon F. Cormier¹

4 ¹Department of Physics, University of Connecticut, 196 Auditorium Road, Storrs, CT 06269, USA

5 *Correspondence to:* Vernon F. Cormier (vernon.cormier@uconn.edu)

6 **Abstract.** The relative contributions of scattering and viscoelastic attenuation to the apparent attenuation of seismic
7 body waves are estimated from synthetic and observed S waves multiply reflected from Earth's surface and the core-
8 mantle boundary. The synthetic seismograms include the effects of viscoelasticity and scattering from small-scale
9 heterogeneity predicted from both global tomography and from thermodynamic models of mantle heterogeneity that
10 have been verified from amplitude coherence measurements of body waves observed at dense arrays. Assuming
11 thermodynamic models provide an estimate of the maximum plausible power of heterogeneity measured by elastic
12 velocity and density fluctuations, we predict a maximum scattering contribution of 43 % to the total measured
13 attenuation of mantle S waves having a dominant frequency of 0.05 Hz. The contributions of scattering in the upper
14 and lower mantle to the total apparent attenuation are estimated to be roughly equal. The relative strength of the
15 coda surrounding observed ScSn waves from deep focus earthquakes is not consistent with a mantle having zero
16 intrinsic attenuation.

17

18 **1 Introduction**

19

20 Seismic tomography reveals a laterally heterogeneous velocity structure in the mantle. Constraining the locations
21 and dimensions of such elastic heterogeneities is critical to understanding the intricate details of the dynamic mixing
22 process of the mantle, which is closely tied to the plate tectonic evolution of the Earth. Large-scale (~ 1000 km)
23 heterogeneities are likely caused by the buoyancy differences that drive thermal-chemical convection. The effects of
24 thermal diffusion, however, limit small-scale (~ 1 to 100 km) heterogeneities to chemical variations. Small-scale
25 heterogeneities can scatter 0.1 to 1 Hz. body waves, transferring energy from body wave pulses observed at a
26 receiver to later time windows and receivers (Shearer, 2015). Mantle attenuation measured from P and S waves will
27 hence always be a summation of a scattering and an intrinsic viscoelastic attenuation. The viscoelastic dispersion of
28 dominantly intrinsic attenuation successfully explains the lower velocities of Earth models derived from low
29 frequency free oscillations observed in the millihertz band from those derived from 1 Hz body waves (Dziewonski
30 and Anderson, 1981). Yet some extrapolations of the scale lengths and intensities of heterogeneity inferred from
31 high frequency body waves have suggested attenuation in the mantle may instead be dominated by scattering
32 (Ricard et al., 2014, Sato, 2019).

33

34 The apparent attenuation of multiple ScS waves is an excellent observable to untangle the relative contributions of
35 scattering and intrinsic attenuation. Many previous studies have used ScS and its reverberations within the mantle to
36 obtain path averaged values for the mantle attenuation. These attenuation measurements are usually represented in
37 terms of a quality factor (Q or Q_{ScS} for ScS-based measurements). The estimates of these apparent attenuation
38 measurements include both the intrinsic or viscoelastic attenuation of the wave amplitude and the attenuation caused
39 by scattering effects. In this work we will consider the apparent attenuation ($\frac{1}{Q_{ScS}}$) to be the addition of intrinsic
40 attenuation ($\frac{1}{Q_{intr}}$) and scattering attenuation ($\frac{1}{Q_{scat}}$) for path averaged observations of SH waves reflected from the
41 free surface and core-mantle boundary. The intrinsic component accounts for the loss of energy due to friction and
42 heat loss as the wave propagates through the mantle with different viscous properties caused by the motion of
43 defects in the crystalline lattice structure of silicates or by the motion of melt at grain boundaries or in pores.
44 Intrinsic attenuation manifests itself in body waves by amplitude decay, pulse broadening, and velocity dispersion.
45 The scattering attenuation accounts for the energy loss that is scattered into different directions as elastic
46 heterogeneities are encountered along the path of a body wave. In addition to amplitude decay and pulse broadening
47 of the main phase, scattering generates increased levels of coda energy comprised of redistributed energy arriving
48 later than the main phase. Many past studies calculating the apparent attenuation of multiple ScS use spectral
49 amplitude ratios (Kovach and Anderson, 1964, Yoshida and Tsujiura, 1975, Sipkin and Jordan, 1980, Lay and
50 Wallace, 1983) and time domain amplitude ratios (Kanamori and Riviera, 2015) of adjacent ScS waveforms. An
51 alternative analysis technique seeks the attenuation operator that converts an ScS_{n-1} waveform into an ScS_n
52 waveform (Jordan and Sipkin, 1977, Revenaugh and Jordan, 1989). Sipkin and Revenaugh (1994) concluded that a
53 frequency domain approach works better for Q_{ScS} measurements, especially in continental regions that tend to have
54 lower shear Q values compared to oceanic regions. Lee et al. (2003) compared observations and numerical
55 simulations of coda envelope offsets before and after ScS synthesized with two-layer scattering models
56 superimposed on a PREM reference model to calculate the scattering contribution to total attenuation measurements.
57 They concluded that scattering loss dominates intrinsic loss in the lower mantle.

58
59 Our effort employs an estimate for a ScS_n attenuation operator to evaluate the relative percentages of scattering and
60 intrinsic attenuation contributing to the apparent attenuation observed from simulated mantle heterogeneity models.
61 Observations of scattered body waves together with geodynamic modeling have established that heterogeneities of
62 scale lengths as small as 4 to 10 km with RMS (root mean square) velocity perturbations of 1 to 8 % can persist
63 throughout the mantle, even in the presence of constant convective stirring (Hedlin et al., 1997, Shearer and Earl,
64 2008, Kaneshima and Helffrich, 2010). Our investigation considers the effects of similar dimensions and
65 perturbation strengths for heterogeneity models. We also consider the effects of a model of mantle heterogeneity
66 power obtained by applying stochastic tomography (Zheng and Wu, 2009) to invert for the heterogeneity spectrum
67 of the upper 1000 km of the mantle from observations of amplitude and phase fluctuations of teleseismic P waves
68 observed by the Earthscope USArray (Cormier, et al.). We assumed fluctuations of S velocity and density to be
69 correlated with those of P velocity such that $\Delta V_S/V_S = 2 \Delta V_P/V_P$ and $\Delta \rho/\rho = 0.8 \Delta V_P/V_P$, taking the resultant depth-

Vernon Cormier 11/11/2019 11:15 AM

Deleted: maximum plausible depth-dependent

Vernon Cormier 11/11/2019 11:16 AM

Deleted: from

De Silva, Manaw..., 11/12/2019 11:47 AM

Deleted: $d \ln V_S / d \ln V_P = 2$

Vernon Cormier 11/11/2019 3:01 PM

Formatted: Subscript

Vernon Cormier 11/11/2019 3:01 PM

Formatted: Subscript

De Silva, Manaw..., 11/12/2019 11:49 AM

Deleted: s

De Silva, Manaw..., 11/12/2019 11:49 AM

Deleted: s

76 [dependent power spectrum to be a maximum plausible model of mantle heterogeneity. With these assumptions, the](#)
77 [power of the heterogeneity spectrum of S velocity closely matches those predicted by thermodynamically](#)
78 [constrained estimates of mantle chemistry and phase. Such models \(e.g., Stixrude and Lithgow-Bertelloni, 2007\)](#)
79 [predict significantly higher heterogeneity than the models of global tomography. Although the assumed chemistry](#)
80 [and potential temperature of thermodynamic models have been shown to affect average mantle velocities, the depth](#)
81 [position of predicted heterogeneity peaks and their maximum power, concentrated around mantle phase transitions,](#)
82 [are relatively unaffected \(Stixrude and Lithgow-Bertelloni, 2012\).](#)

84 2 Method

86 2.1 Models

88 Apparent attenuations are measured from ScSn waveforms observed in synthetic seismograms for 4 different models
89 of mantle heterogeneity. All of these assume PREM as the one dimensional background velocity and density model,
90 with the PREM shear wave attenuations providing the purely intrinsic component of attenuation. Model 1 does not
91 perturb PREM with any lateral heterogeneities. Therefore, the apparent attenuation measured for this case will be
92 purely intrinsic. Model 2 (Fig.1) applies a depth-dependent shear velocity perturbation to the PREM mantle similar
93 to those determined from many seismic tomographic studies (Megnin and Romanowicz, 2000, Ritsema et al., 2004).
94 Model 3 (Fig. 2) applies [scaled shear velocity and density perturbations to the PREM mantle based on the stochastic](#)
95 [P tomography model of Cormier et al. \(2019\)](#) for the upper 1000 km of the mantle. Model 4 (Fig. 3) is the same as
96 Model 3 in the upper 1000 km of the mantle but includes an additional peak in heterogeneity power in the
97 lowermost mantle predicted [by Stixrude and Lithgow-Bertelloni \(2012\)](#) from the effect of the post-perovskite phase
98 transition. In Model 5, the intrinsic attenuations are turned off while still applying the thermodynamic model of
99 mantle heterogeneity to shear velocity perturbations. Hence the synthetic seismograms for this model will exhibit
100 purely scattering effects in any attenuation measurement. In all models, heterogeneities are represented as stochastic
101 random media with an exponential autocorrelation having a corner scale equal to 10 km. In Models 2, 3, 4, and 5 we
102 assume a relation between [P velocity and density and shear velocity perturbations such that \$\Delta\rho/\rho = 0.8 \Delta V_p/V_p\$](#)
103 [and \$\Delta V_s/V_s = 2 \Delta V_p/V_p\$](#) . The value for density perturbation in a mantle close to neutral buoyancy is relatively large,
104 but is commonly assumed in studies of crustal and upper mantle scattering based on Birch's law (Birch, 1952).

106 2.2 Apparent attenuation measurements

108 All simulations are performed by a numerical pseudospectral method in 2-D (Cormier, 2000), assuming an SH line
109 source at 500 km depth with a Gaussian-shaped source-time function having a half-width of 1.2 seconds. Wave
110 propagation uses a 2D staggered grid of radial step size 3.0 km and lateral step size 5.427 km, with time sampling
111 set to 0.025 seconds ensuring stability and negligible grid dispersion. Intrinsic attenuation, taken to be
112 approximately constant across a broad frequency band, is introduced by three memory functions using the methods

Vernon Cormier 11/11/2019 11:46 AM

Deleted:

Vernon Cormier 11/11/2019 11:31 AM

Deleted: γ (Stixrude and Lithgow-Bertelloni, 2007, Stixrude and Lithgow-Bertelloni, 2012). We have recently validated (Cormier et al., 2019) a thermodynamic model of mantle heterogeneity by applying stochastic tomography (Zheng and Wu, 2008) to the upper 1000 km of the mantle to invert for amplitude and phase fluctuations observed by the US transportable array. Assessing the scattering attenuation induced by thermodynamic models, which predict heterogeneity to be concentrated in mantle phase transition zones, can assist in quantifying mantle heterogeneity and testing for the existence of additional phase transitions.

Vernon Cormier 11/11/2019 12:01 PM

Deleted: a

Vernon Cormier 11/11/2019 11:57 AM

Deleted: similar to the

Vernon Cormier 11/11/2019 11:59 AM

Deleted: predictions of thermodynamic studies

Vernon Cormier 11/11/2019 11:59 AM

Deleted: (Stixrude and Lithgow-Bert... [1])

Vernon Cormier 11/11/2019 2:57 PM

Deleted: $\delta\lambda\gamma$

Vernon Cormier 11/11/2019 2:58 PM

Formatted: Font:Symbol

De Silva, Manaw..., 11/12/2019 11:49 AM

Deleted: s

De Silva, Manaw..., 11/12/2019 11:49 AM

Deleted: s

Vernon Cormier 11/11/2019 2:58 PM

Formatted: Font:Symbol

Vernon Cormier 11/11/2019 2:58 PM

Deleted:

Vernon Cormier 11/11/2019 3:00 PM

Formatted: Subscript

Vernon Cormier 11/11/2019 2:59 PM

Deleted: $d\ln V_s/V_s$

Vernon Cormier 11/11/2019 12:02 PM

Deleted: is

Vernon Cormier 11/11/2019 3:00 PM

Formatted: Subscript

Vernon Cormier 11/11/2019 3:00 PM

Formatted: Subscript

Vernon Cormier 11/11/2019 3:00 PM

Formatted: Subscript

143 described by Robertson et al., (1994). Waveforms are computed at a great circle distance of 18° in order to avoid
 144 contamination of ScSn phases with depth phases or other nearby arrivals. These are corrected for 3D geometric
 145 spreading, and a line-to-point source conversion is made. [Although 2D and 2.5D simulations neglect the effects of](#)
 146 [out-of-plane scattering, a comparison of 2-5D with 3D scattering simulations by Wu and Irving \(2017\) suggests that](#)
 147 [the neglect of out-of-plane scattering on the coda of teleseismic body waves are small.](#) For each of the 5 models a 2-
 148 parameter attenuation operator (Eq. 1) is determined that converts the ScS waveform into an ScSScS waveform.
 149 Each attenuation operator depends on Q_{ScS} and the high frequency corner ($1/\tau_m$) of a relaxation spectrum, where
 150 attenuation is constant for 5 decades of frequency.

151 In the inversion procedure, the predicted ScSScS velocity waveform is generated by convolving the ScS waveform
 152 with an attenuation operator corresponding to a peak attenuation $1/Q_{ScS}$ and a high frequency corner $1/\tau_m$. A least
 153 squares norm is calculated (Eq. 2) for the difference between observed and predicted ScSScS velocity waveforms,
 154 which are aligned by the arrival times of first maximum and normalized by the peak-to-trough amplitudes (Fig. 4).
 155 A search over the two attenuation parameters is then performed to minimize an L2 norm difference to maximize a
 156 Gaussian probability density constructed using the L2 norm difference (Cormier et al., 1998). Half-widths of the
 157 probability density functions are used to infer errors.

158
 159 An operator to convert an ScS waveform into an ScSScS waveform is defined in the frequency domain by
 160

$$161 \quad O(\omega, Q, \tau) = \exp(-i\omega[\int_{ScSScS} \frac{ds}{\hat{v}(\omega)} - \int_{ScS} \frac{ds}{\hat{v}(\omega)}]) \quad (1)$$

162 where

$$\hat{v}(\omega, Q, \tau) = \frac{\sqrt{1 + \frac{2}{\pi Q_{ScS}^{-1} \ln\left(\frac{-i\omega + 1/\tau_l}{-i\omega + 1/\tau_m}\right)}}}{\sqrt{1 + \frac{2}{\pi Q_{ScS}^{-1} \ln\left(\frac{-i2\pi + 1/\tau_l}{-i2\pi + 1/\tau_m}\right)}}$$

163 and where

164 τ_l is the period of the low frequency corner in relaxation spectrum and $\frac{\tau_l}{\tau_m} = 10^5$

165 The least squares norm difference between observed and predicted waveforms is calculated from

$$166 \quad L2N(Obs, Pred) = \sqrt{\sum_t \frac{(Amp_{obs}(t) - Amp_{pred}(t))^2}{\sigma^2}} \quad (2)$$

168 where σ is a $\frac{noise}{signal}$ measurement from a 100 second time window preceding the ScSScS observation.

169

170 Our goal was to simply estimate an apparent attenuation parameter Q_{ScS} for the whole of the mantle when the effects
 171 of scattering are included rather than to seek a best fitting depth and frequency dependent attenuation model.

172 Accurate separation of depth from frequency dependence of attenuation benefits from observations of S and ScS
173 over a range of source depths and distances as well as by an analysis of P waves to sample a broader frequency
174 band. Nonetheless, our estimates for the high frequency corner parameter $1/\tau_m$ were bounded by estimates for $1/\tau_m$
175 in the upper and lower mantle found by Choy and Cormier (1986).

177 3. Results

178
179 We found MODEL 1, which has pure intrinsic attenuation and no small-scale heterogeneity, to have an apparent
180 attenuation value of 0.004167 corresponding to a $Q_{ScS} = 240$. This estimated Q_{ScS} value differs by only 2.2 % from
181 the theoretical estimate of the depth averaged Q_{ScS} obtained for PREM with the relation $Q_{ScS} = (\int_{x_{ScSScS}} dt -$
182 $\int_{x_{ScS}} dt) / (\int_{x_{ScSScS}} dt / Q_s(x) - \int_{x_{ScS}} dt / Q_s(x))$. Here x_{ScSScS} and x_{ScS} denote points along the path of
183 ScSScS and ScS respectively, $Q_s(x)$ denote the Q_s values at those points read from 1D PREM. This result verifies
184 the accuracy of the waveform L2 norm method for estimating Q_{ScS} .

185
186 With MODEL 2, which has a conventional tomographic estimate of mantle heterogeneity, we find that the apparent
187 attenuation is increased to 0.005 (Q_{ScS} decreased to 200). Together with the knowledge of the purely intrinsic
188 contribution ($\frac{1}{Q_{intr}}$) calculated in MODEL 1, the scattering component of attenuation ($\frac{1}{Q_{scat}}$) in MODEL 2 is
189 estimated to be 0.000833. Hence the scattering caused by small-scale (~ 10 km) heterogeneities with a dV_s/V_s depth
190 profile similar to S20RTS (Ritsema et al., 2004), would account for 16.7 % of the measured ScS apparent
191 attenuation. MODEL 3, which has a higher amount of heterogeneity due to increased V_s perturbations associated
192 with predicted lateral variations in phase changes in the upper mantle, results in a higher apparent attenuation of
193 0.005747 ($Q_{ScS} = 174$). MODEL 4, which includes additional heterogeneity predicted for the effects of a post-
194 perovskite phase transition results in an even higher apparent attenuation of 0.007100 ($Q_{ScS} = 140$). We calculate
195 that the scattering attenuation in the lower mantle (below 1000 km) and upper mantle (above 1000 km) of MODEL
196 4 to be 0.0014 and 0.0016 with their percent contributions to the total apparent attenuation being 19.6 % and 22.4 %
197 respectively. The overall scattering attenuation of MODEL 4 is 0.002933 with the scattering component accounting
198 for 41.3 % of the measured ScS total apparent attenuation.

199 Finally, in MODEL 5 the intrinsic attenuation in the mantle is turned off while applying the mantle heterogeneity of
200 MODEL 4. The apparent attenuation (now purely due to scattering) is measured to be 0.0029 ($Q_{ScS} = 340$). This high
201 Q value lies towards the upper bound of regional estimates (~ 360) of Q_{ScS} (Nakanishi, 1979, Sipkin & Revenaugh
202 1994, Gomer & Okal, 2003). It is also found that apparent attenuation measurements of MODEL 5 and MODEL 1
203 add up to be exactly equal to MODEL 4, validating the attenuation estimation method in conjunction with the
204 assumption of $\frac{1}{Q_{apparent}} = \frac{1}{Q_{intr+scat}} = \frac{1}{Q_{intr}} + \frac{1}{Q_{scat}}$.

205
206 Figure 6 compares the levels of scattered coda energy arriving in the vicinity (~ ± 150 s) of the ScSScS main arrival
207 generated by different models of mantle heterogeneity models to the synthetic ScSScS predicted by MODEL 1

- De Silva, Manaw..., 11/12/2019 11:55 AM
- Deleted: band
- Vernon Cormier 11/11/2019 12:09 PM
- Deleted:
- Vernon Cormier 11/11/2019 12:14 PM
- Deleted: O
- Vernon Cormier 11/11/2019 12:14 PM
- Deleted: ,
- Vernon Cormier 11/11/2019 3:14 PM
- Deleted: within the range
- Vernon Cormier 11/11/2019 3:14 PM
- Deleted: the
- Vernon Cormier 11/11/2019 3:15 PM
- Deleted: in the study

215 having no scattering. Observing the envelopes of squared velocity for MODEL 2 versus MODEL 4, it is apparent
216 that the levels of energy arriving in the coda and before the main phase significantly increase and the ScSScS pulse
217 width increases due to the presence of increased small-scale heterogeneity in the regions associated with mantle
218 phase changes. It also is important to recognize that intrinsic attenuation can affect the ratio of coda energy to the
219 main pulse. The results for MODEL 5, which omits intrinsic attenuation, demonstrate the importance of intrinsic
220 attenuation for the coda as well as the direct phases. In this case the coda, unaffected by intrinsic attenuation,
221 approaches the amplitude of the direct ScSScS phase.

222

223 4. Discussion

224

225 4.1 Comparison with regional variations

226 To obtain recordings of clear ScS and ScSScS without interference by depth phases and other arrivals (S, SS, sS),
227 we searched for waveforms of deep focus events in the 10° to 30° distance with moment magnitude > 6 Mw. In
228 supplement Fig. S1 we plot such events available in catalogues of the IRIS DMC from 1970-01-01 to 2019-11-07.
229 The analysis of the waveforms and their codas in the full data set satisfying these conditions would be quite valuable
230 to better constrain predictions regarding the real mantle. The main objective of this study, however, was to a
231 describe a well-defined modeling method and to illustrate how this modeling may be used to constrain the mantle
232 heterogeneity spectrum from ScS and ScSScS waveforms with several observations representative of the range of
233 measured attenuations.

234 Regional variations measured for Q_{ScS} generally fall in the range of 140 – 360 (Nakanishi, 1979, Sipkin &
235 Revenaugh, 1994, Gomer & Okal 2003). Variations on this order are confirmed when we apply our inversion
236 method to two example multiple ScS observations observed from deep focus earthquakes (Fig. 7). We obtain $Q_{ScS} =$
237 153 for an earthquake beneath Papua New Guinea region observed at a station located at Charters Towers in
238 Australia, and $Q_{ScS} = 200$ for an earthquake beneath the eastern China-Russia border region observed at a station
239 located at Yakutsk in eastern Siberia. In Fig. 8 we overlay synthetic seismograms computed from several of our
240 models to determine of how scattering in combination with intrinsic attenuation can affect the relative amplitudes of
241 the direct ScSScS phase and its coda. The heterogeneity power of MODEL 2 inferred from global tomography is too
242 weak to match the excitation of coda relative to ScSScS in both our data examples. Conventional tomographic
243 models typically underestimate true perturbation intensities through the effects of regularization parameters that
244 smooth over the effects of more intense and unresolvable small-scale heterogeneity (e.g., Ritsema et al., 2007).
245 MODEL 4, having PREM attenuation and heterogeneity predicted for a thermodynamic model of the mantle, best
246 matches the relative coda and direct phase excitations for both events. The match can be improved by either a small
247 decrease in intrinsic attenuation or a small increase in heterogeneity power for the eastern China-Russia border
248 region to Yakutsk. ScSn paths from both earthquakes traverse a region of the mantle on the back-arc side of dipping
249 slabs, a southwest dipping slab toward the Australian craton in the case of the New Guinea event (Tregoning and
250 Gorbatov, 2004), and a western dipping Kuril-Kamchatka slab (Koulakov et al., 2011) toward the Siberian craton in

Vernon Cormier 11/11/2019 4:56 PM

Deleted:

Vernon Cormier 11/11/2019 4:55 PM

Formatted: Font:10 pt

De Silva, Manaw..., 11/12/2019 12:04 PM

Formatted: Normal (Web), Left

Vernon Cormier 11/11/2019 4:55 PM

Formatted: Font:Not Bold

Vernon Cormier 11/11/2019 3:19 PM

Deleted:

253 the case of the eastern China-Russia border event. The multiple ScSn paths for the eastern China-Russia border
254 event are more slab parallel and distant from the descending slab and more strongly sample the cratonic upper
255 mantle compared to the New Guinea event. Hence, it is likely that the intrinsic attenuation of PREM overestimates
256 the effects of mantle attenuation on ScSn's. Finally, a comparison of observations with the prediction of Model 5,
257 having no intrinsic attenuation, over-predicts coda excitation relative to ScSScS for both events. This confirms that
258 some intrinsic attenuation in the mantle is necessary to dampen the coda generated by the most extreme plausible
259 suggestions of heterogeneity power.

260

261 **4.2 Upper and lower mantle scattering and intrinsic attenuation**

262

263 Strong depth dependence of mantle attenuation, both intrinsic and scattering, has long been documented. Intrinsic
264 attenuation has been found to be relatively low in the mid and deep mantle compared to the upper mantle. Evidence
265 of some scattering in the mid and deep mantle has been confirmed in studies of PKIKP precursors in the 120° to
266 140° great circle range (e.g., Hedlin et al., 1997), including strong regional and depth variations that may be
267 consistent with the effects of either remnant subducted oceanic crust or with a peak in heterogeneity power
268 associated with a post-perovskite phase change. From a study of S and ScS coda, Lee et al. (2003) estimated that
269 scattering attenuation dominates intrinsic attenuation in the lower mantle, reporting their results in terms of the
270 scattering coefficients for a two-layered model of mantle heterogeneity. The scattering coefficients g are related to
271 scattering attenuation by $g = \omega / (Q_{\text{scat}} V_s)$. Our results for MODEL 3 and MODEL 4 show that seismic albedo,
272 the ratio of scattering loss to total attenuation, below 1000 km depth in the mantle is 30 % while above 1000 km it is
273 27 %. This is assuming the PREM average intrinsic shear Q of 225 and 312 for the two depth regions. Hence, we do
274 not observe the scattering to dominate over intrinsic effects in either lower or upper mantle, although regional
275 exceptions can be expected. Additionally, considering the estimated scattering attenuations for MODEL 3 and
276 MODEL 4, we can deduce the scattering coefficients to be $6.25 \times 10^{-5} \text{ km}^{-1}$ for the mantle below 1000 km and 1.256
277 $\times 10^{-4} \text{ km}^{-1}$ for mantle above 1000 km in MODEL 4. These scattering coefficients, calculated for a dominant
278 frequency of 0.05 Hz, are comparable to the low frequency estimates of Lee et al. (2003). This result implies a
279 relatively lower scattering coefficient (i.e. slightly lower scattering attenuation) in the lower mantle compared to the
280 upper mantle in MODEL 4, which agrees with the Lee et al. estimates of scattering coefficients.

281

282 **4.3 Origins of heterogeneity and scale length anisotropy**

283

284 In suggesting that scattering attenuation may dominate intrinsic attenuation throughout the mantle Ricard et al.
285 (2014) considered the effects of heterogeneity distributed primarily in the form of horizontal layers based on
286 geodynamic numerical experiments that predict folding and horizontal stretching of chemical heterogeneity (e.g.,
287 Manga, 1996) whose origin primarily originates from the convective cycling of oceanic crust. The attenuative
288 effects of horizontally layered structure have been well known since the classic paper by O'Doherty and Anstey
289 (1971) and are simply calculated. In this paper, we have instead considered the effects of scale lengths predicted by

290 thermodynamic models in which variations in temperature and chemistry dictate the stability of silicate mineral
291 phases. These variations in temperature and chemistry can also be connected to the convective cycling of oceanic
292 crust, but instead predict that peaks in heterogeneity power will be concentrated near phase transitions. Such models
293 have not yet fully considered the effects of mechanical mixing on the anisotropy of scale lengths within these
294 relatively narrow regions of depth. Nonetheless, thermodynamic models, when verified by observations of scattering
295 effects that supplement tomographic imaging, may at least provide a more reliable estimate of the upper bound to
296 velocity and density fluctuations in the mantle. Experiments similar to ours may be extended to include the effects
297 of anisotropy of scale lengths. Our results indicate that some intrinsic attenuation will always be required to explain
298 the attenuation of body waves, regardless of the state of isotropy of scale lengths.

299

300 **5. Conclusions**

301

302 An inversion algorithm for apparent mantle attenuation based on L2 norm differences between observed and
303 predicted ScSScS velocity waveforms has been verified by inversion of synthetic seismograms and applied to
304 estimate the relative contributions of intrinsic and scattering attenuation to the total apparent attenuation.
305 Thermodynamic models of mantle heterogeneity predict significantly higher heterogeneity power than the
306 predictions from global tomography, and a correspondingly higher relative contribution to apparent attenuation
307 measured from body waves. Taking the depth-dependent heterogeneity power of thermodynamic models of mantle
308 heterogeneity as the maximum plausible heterogeneity we estimate that scattering may explain up to 41.3 % of
309 apparent mantle attenuation with up to 3 % RMS shear velocity perturbations concentrated near mantle phase
310 transitions and 1 % everywhere else. We estimate the scattering contribution to the apparent attenuation from
311 heterogeneity in the upper and lower mantle to be roughly equal in global averages, but regional variations between
312 upper and lower mantle scattering contributions are likely. These estimates agree well with the excitation of coda
313 surrounding ScSn waves observed from deep focus earthquakes. These codas can only be matched by the existence
314 of both intrinsic and scattering attenuation.

315

316 **Data Availability.** The data set of SH component synthetic seismograms can be found at
317 <https://doi.org/10.5281/zenodo.3460694> (Desilva and Cormier, 2019).

318

319 **Acknowledgements.** This work was supported by grants EAR 14-46509 from the National Science Foundation.

320

321 **References**

322

323 Birch F.: Elasticity and constitution of the Earth's interior, *J. Geophys. Res.* 57, 227–286, 1952..

324 Choy, G., and Cormier, V.F.: Direct measurement of the mantle attenuation operator from broadband P and S
325 waves, *J. Geophys. Res.* 91, 7326-7342, 1986.

326 Cormier, V., Li, X., and Choy, G.: Seismic attenuation of the inner core: Viscoelastic or stratigraphic?, *Geophysical*
327 *Research Letters*, 25 (21), 4019-4022, 1998.

328 Cormier, V. F.: D'' as a transition in the heterogeneity spectrum of the lowermost mantle, *Journal of Geophysical*
329 *Research: Solid Earth*, 105(B7), 16193-16205, 2000.

330 Cormier, V.,F., Tian, Y., and Zheng, Y.: Heterogeneity spectrum of Earth's upper mantle obtained from the
331 coherence of teleseismic P waves, *Communications in Computational Physics*, 26(5), 1-27, doi: 10.4208/cicp.OA-
332 2018-079, 2019.

333 Desilva, S. and Cormier, V.: SH component synthetic seismograms (SE_Supplementary_data) (Version v1.0.0)
334 [Data set]. Zenodo. <http://doi.org/10.5281/zenodo.3460695>, 2019.

335 Dziewonski, A. D. and Anderson, D. L.: Preliminary reference earth Model, *Phys. Earth Planet. Inter.*, 25, 297-356,
336 1981.

337 Gomer, B., and Okal, E.: Multiple-Scs probing of the Ontong-Java Plateau, *Physics of the Earth and Planetary*
338 *Interiors*, 138(3-4), 317-331, 2003.

339 Hedlin M A, Shearer P, and Earle P.: Seismic evidence for small-scale heterogeneity throughout the Earth's mantle,
340 *Nature*, 387(6629), 145-150, 1997.

341 Jordan, T. H., and Sipkin S. A.: Estimates of the attenuation operator for multiple ScS Waves, *Geophysical Research*
342 *Letters*, 4(4), 167-170, 1977.

343 Kanamori, H., and Rivera, L.: Nearvertical multiple ScS phases and vertically averaged mantle properties,
344 *interdisciplinary Earth: A Volume in Honor of Don L. Anderson: Geological Society of America Special Paper*, 514
345 and *American Geophysical Union Special Publication*, 71, 9–31, 2015.

346 Kaneshima, S., and Helffrich, G.: Small scale heterogeneity in the mid-lower mantle beneath the circum-Pacific
347 area, *Physics of the Earth and Planetary Interiors*, 183(1-2), 91-103, 2010.

348 Kovach, R. L., and Anderson, D. L.: Attenuation of shear waves in the upper and lower mantle, *Bulletin of the*
349 *Seismological Society of America*, 54(6A), 1855-1864, 1964.

350 Koulakov, I.Y., Dobretsov, N.L., Bushenkova, N.A., and Yakovlev, A.V.: Slab shape in subduction zones beneath
351 the Kurile-Kamchatka and Aleutian arcs based on regional tomography results, *Russ. Geol. and Geophys*, 52, 650-
352 667, 2011.

353 Lay, T., and Wallace, C.: Multiple scs travel times and attenuation beneath mexico and central america, *Geophysical*
354 *Research Letters* , 10(4), 301-304, 1983.

355 Lee, W., Sato, H., and Lee, K.: Estimation of S-wave scattering coefficient in the mantle from envelope
356 characteristics before and after the ScS arrival, *Geophysical Research Letters*, 30(24), 1-5, 2003.

357 Manga, M.: Mixing of heterogeneities in the mantle: Effect of viscosity differences, *Geophysical Research Letters*,
358 23(4), 403-406, doi: 10.1029/96GL00242, 1996.

359 Megnin, C., and Romanowicz, B.: The three-dimensional shear velocity structure of the mantle from the inversion of
360 body, surface and higher-mode waveforms, *Geophysical Journal International*, 143, 709-728, 2000.

361 Nakanishi, I.: Attenuation of multiple ScS waves beneath the Japanese arc, *Physics of the Earth and Planetary*
362 *Interiors*, 19(4), 337-347, 1979.

363 O'Doherty, R. F. and Anstey, N. A.: Reflections on amplitudes, *Geophys. Prosp.*, 19, 430- 458, 1971.

364 Revenaugh, J., and Jordan, T.: A study of mantle layering beneath the western Pacific, *Journal of Geophysical*
365 *Research*, 94(B5), 5787-5813, 1989.

366 Ricard, Y., Durand, S., Montagner, J., and Chambat, F.: Is there seismic attenuation in the mantle?, *Earth and*
367 *Planetary Science Letters*, 388, 257-264, 2014.

368 Ritsema, J., van Heijst, H., and Woodhouse, J.: Global transition zone tomography, *Journal of Geophysical*
369 *Research: Solid Earth*, 109(B2) , 2004.

370 [Ritsema, J., McNamara, A.K., Bull, A.L., Tomographic filtering of geodynamic models: Implications for model](#)
371 [interpretation and large-scale mantle structure, *J. Geophys. Res.*, doi: 10.1028/2006JB004566, 2007.](#)

372 Robertson, J.O.A., Blanch, J.O., and Symes, W.W.: Viscoelastic finite-difference modeling, *Geophysics*, 58. 1444-
373 1456, 1994.

374 Sato, H.: Power spectra of random heterogeneities in the solid earth, *Solid Earth*, 10, 275-292, 2019.

375 Shearer, P.: Seismic scattering in the deep Earth, *Treatise on Geophysics Second Edition*, 1, 759-787, 2015.

376 Shearer, P., and Earle, P.: Observing and Modeling Elastic Scattering in the Deep Earth, *Advances in Geophysics*,
377 50(08), 167-193, 2008.

378 Sipkin, S., and Jordan, T.: Regional variation of Qscs, *Bulletin of the Seismological Society of America*, 70 (4),
379 1071-1102, 1980.

380 Sipkin, S., and Revenaugh, J.: Regional variation of attenuation and travel time in China from analysis of multiple-
381 ScS phases, *Journal of Geophysical Research*, 99(B2), 2687-2699, 1994.

382 Stixrude, L., and Lithgow-Bertelloni, C.: Influence of phase transformations on lateral heterogeneities and dynamics
383 in Earth's mantle, *Earth Planet. Sci. Lett.*, 263, 45-55, 2007.

384 Stixrude, L., and Lithgow-Bertelloni, C.: Geophysics of Chemical Heterogeneity in the Mantle, *Annual Review of*
385 *Earth and Planetary Sciences*, 40(1), 569-595, 2012.

386 Tregoning, P., and Gorbатов, A.: Evidence for active subduction at the New Guinea Trench, *Geophys. Res. Lett.*,
387 doi: 10.1029/2004GL020190, 2004.

388 Yoshida, M., and Tsujiura, M.: Spectrum and attenuation of multiply reflected core phases, *Journal of Physics of the*
389 *Earth*, 23(1), 31-42, 1975.

Vernon Cormier 11/11/2019 4:56 PM
Formatted: Font:10 pt, Not Bold, Font color: Text 1

Vernon Cormier 11/11/2019 4:56 PM
Formatted: Heading 1, Line spacing: double

Vernon Cormier 11/11/2019 4:56 PM
Formatted: Font:10 pt, Not Bold

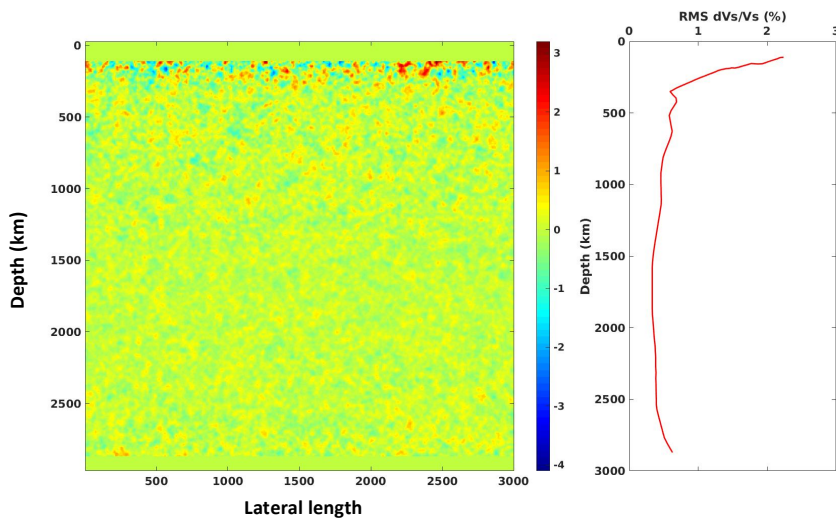
Vernon Cormier 11/11/2019 4:56 PM
Formatted: Font:Font color: Text 1

390 [Wu, W., and Irving, J., Using PKiKP coda to study heterogeneity in the top layer of the inner core's western](#)
391 [hemisphere, *Geophys. J. Int.*, 209, 672-687, 2017.](#)

392 [Zheng, Y., and Wu, R.: Theory of transmission fluctuations in random media with a depth-dependent background](#)
393 [velocity structure, *Advances in Geophysics*, 50, 21-41, 2008.](#)

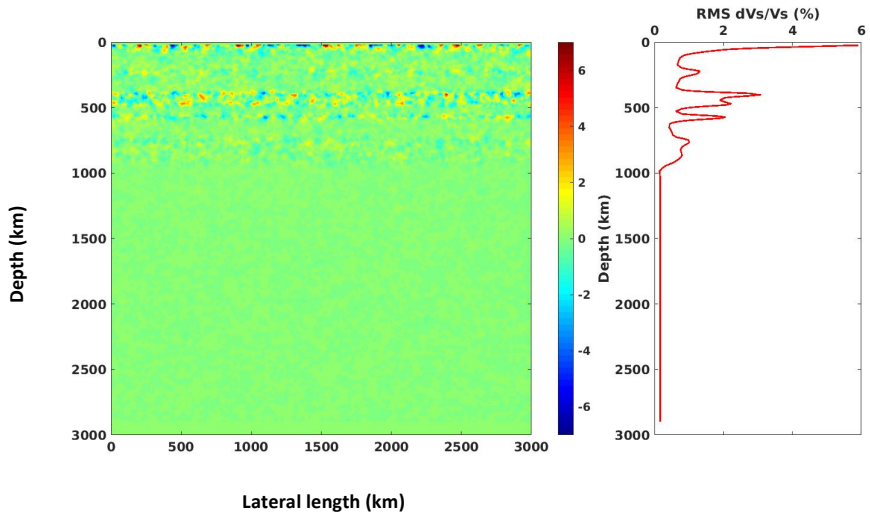
- Vernon Cormier 11/11/2019 4:57 PM
Formatted: Font:10 pt, Not Bold
- Vernon Cormier 11/11/2019 4:57 PM
Formatted: Line spacing: double
- Vernon Cormier 11/11/2019 4:57 PM
Formatted: Font:10 pt
- Vernon Cormier 11/11/2019 4:57 PM
Formatted: Font:10 pt, Not Bold
- Vernon Cormier 11/11/2019 3:40 PM
Formatted: Font:12 pt, Check spelling and grammar
- Vernon Cormier 11/11/2019 3:39 PM
Formatted: Normal, Line spacing: single

395
396
397
398
399
400
401
402
403
404
405
406
407
408
409
410
411
412
413
414
415
416
417
418



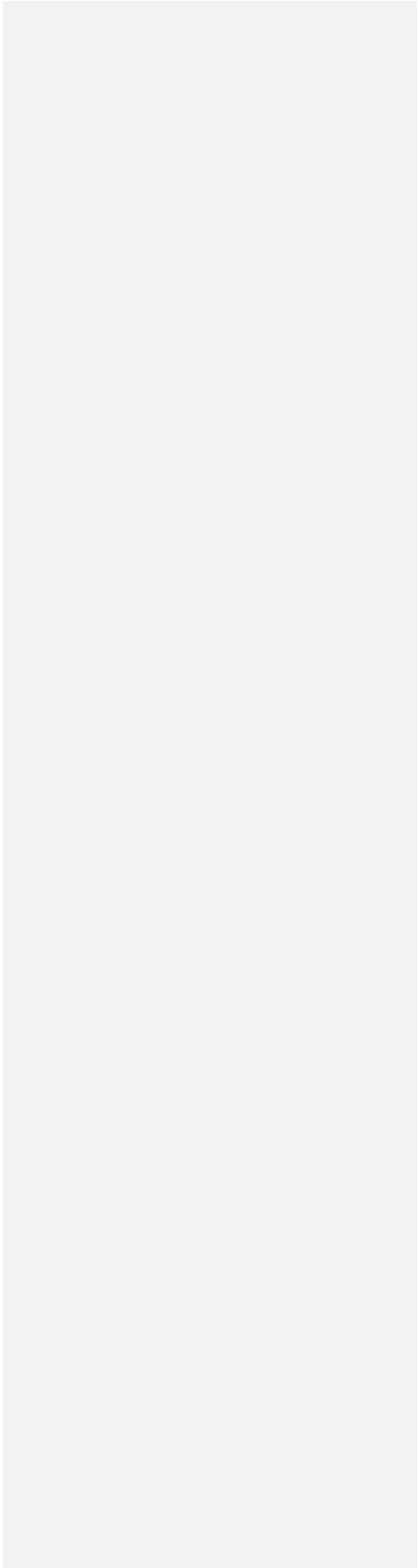
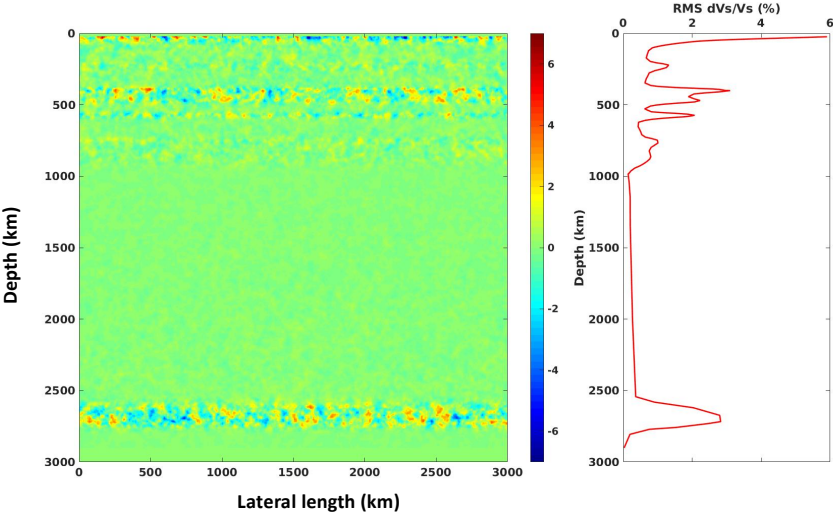
419
420
421
422
423
424
425
426
427
428
429
430
431
432
433
434
435
436
437
438
439
440
441
442
443
444
445
446
447
448
449
450
451
452
453
454
455
456
457
458
459

Figure 1: Right: depth dependent RMS shear velocity perturbation profile applied in Model 2. This is extracted from S20RTS. Left: 2D representation of the same depth dependent profile. Heterogeneous media is for an exponential autocorrelation (corner scale $a = 10$ km) function. Note the increase in heterogeneity power near the top and bottom of the mantle.



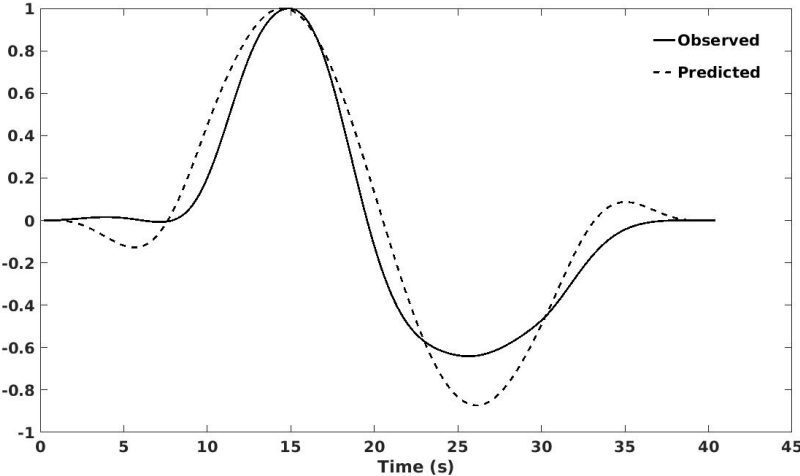
460
461
462
463
464
465
466
467
468
469
470
471
472
473
474
475
476
477
478
479
480
481
482
483
484
485
486
487
488
489
490
491
492
493
494
495
496
497
498
499
500

Figure 2: Right: Depth dependent RMS shear velocity perturbation profile applied in Model 3 vs. perturbation values from crust to 1000 km depth is extracted from the stochastic tomography result of Cormier et al. (2019). Left: 2D representation of the same depth dependent profile. Compared to Model 2 note the additional peaks in heterogeneity power associated with phase transitions in the upper mantle.



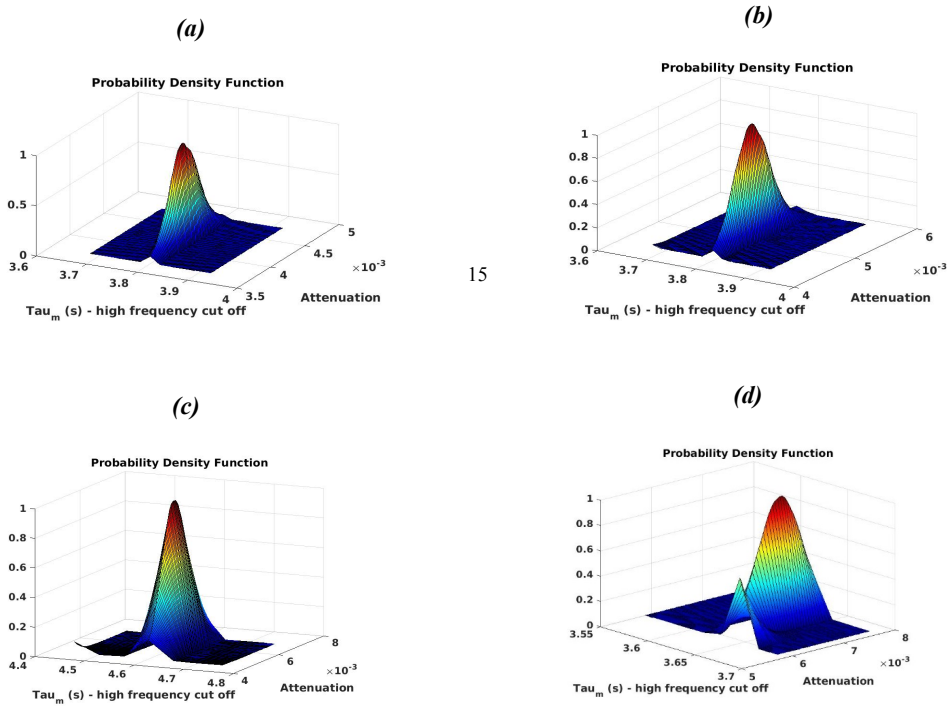
501
502
503
504
505
506
507
508
509
510
511
512
513
514
515
516
517
518
519
520
521
522
523
524
525
526
527
528
529
530
531
532
533
534
535
536
537
538
539
540
541

Figure 3: Right: Depth dependent RMS shear velocity perturbation profile applied in Model 4 vs. perturbation values from crust to 1000 km depth is extracted from the stochastic tomography result of Cormier et al. (2019). Compared to Model 3 an additional peak is added near the core mantle boundary to incorporate the increased lower mantle associated with the post-perovskite phase change (Stixrude & Lithgow-Bertelloni, 2012) Left: 2D representation of the same depth dependent profile.



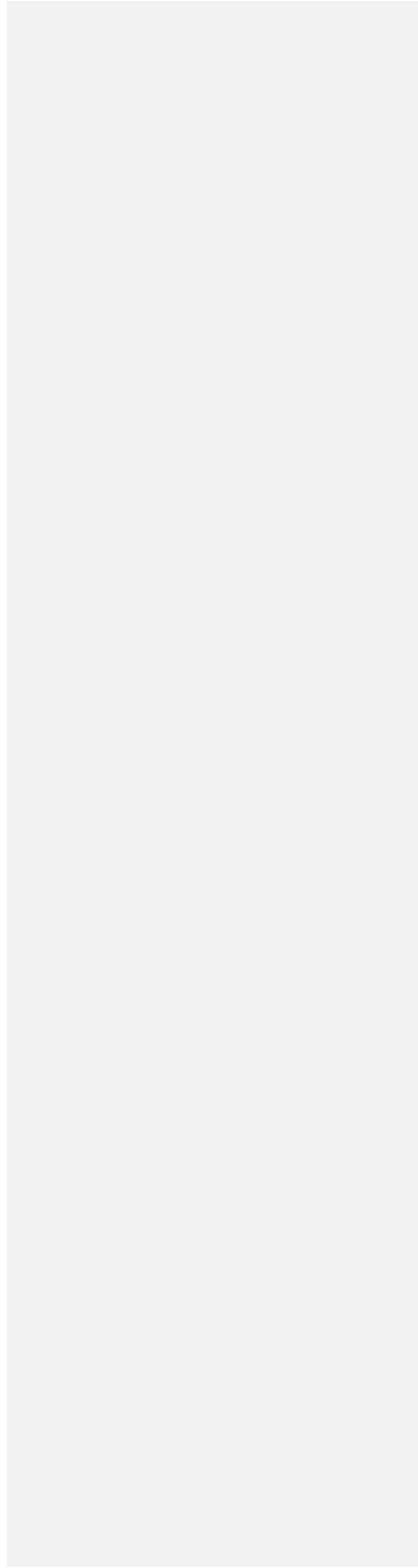
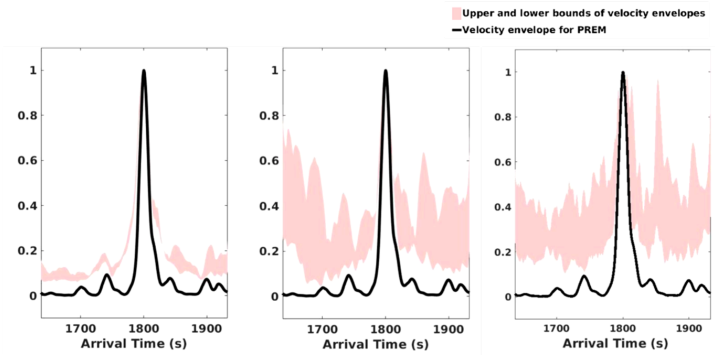
542
543
544
545
546
547
548
549
550
551
552
553
554
555
556
557
558
559
560
561
562
563
564
565
566
567
568
569
570
571
572
573
574
575
576
577
578
579
580
581
582
583

Figure 4: Observed and predicted ScSScS velocity waveform aligned by the arrival time of first extremum and normalized by the peak to trough amplitude. The least squares norm difference between these two waveforms is obtained using a summation of amplitude differences over time.



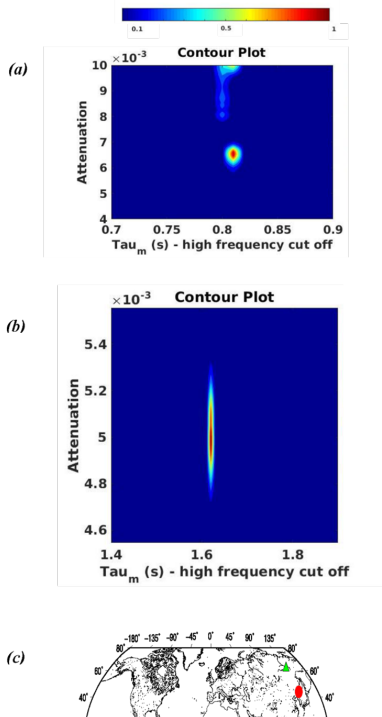
584
585
586
587
588
589
590
591
592
593
594
595
596
597
598
599
600
601
602
603
604
605
606
607
608
609
610
611
612
613
614
615
616
617
618
619
620
621
622
623
624

Figure 5: Gaussian probability density function constructed with the least squares norm difference between predictions and simulated observations for (a) MODEL 1, (b) MODEL 2, (c) MODEL 3, (d) MODEL 4 and (e) MODEL 5.



625
626
627
628
629
630
631
632
633
634
635
636
637
638
639
640
641
642
643
644
645
646
647
648
649
650
651
652
653
654
655
656
657
658
659
660
661
662
663
664
665
666

Figure 6: Upper-lower bounds of coda envelopes (shaded area) calculated from 5 random heterogeneity realizations of each MODEL 2 (left), MODEL 4 (middle) and MODEL 5 (right), compared to PREM (black line).



667
668
669
670
671
672
673
674
675
676
677
678
679
680
681
682
683
684
685
686
687
688
689
690
691
692
693
694
695
696
697
698
699
700
701

Figure 7: Contour plots of probability density functions obtained with multiple ScS observations in two regions. Event (circles) and IU station (triangles) locations for the two regions described below are shown in panel (c).

- (a) **Mantle beneath Papua New Guinea region : Observations are recorded by station CTAO (146.25° E, 20.08° S) for a 490 km deep, mw 6.6 event (154.88° E, 45.43° S) which occurred on May 02 1998, 13:34:28 UTC. Event-station distance is 17.6°.**
- (b) **Mantle beneath Eastern China-Russia border region : Observations are recorded by station YAK (129.68° E, 62.03° N) for a 568 km deep, mw 7.3 event (130.66° E, 43.76° N) which occurred on June 28 2002, 17:19:30 UTC. Event-station distance is 18.3°.**

702
 703
 704
 705
 706
 707
 708
 709
 710
 711
 712
 713
 714
 715
 716
 717
 718
 719
 720
 721
 722
 723
 724
 725
 726
 727
 728
 729
 730
 731
 732
 733
 734
 735
 736
 737
 738
 739
 740
 741
 742
 743

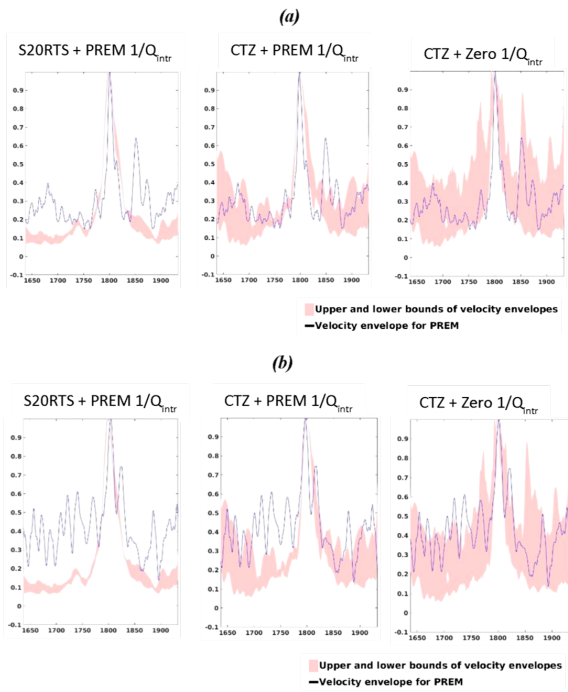


Figure 8: Upper-lower bounds of coda envelopes (shaded area) calculated from 5 random heterogeneity realizations of each MODEL 2 (left), MODEL 4 (middle) and MODEL 5 (right), compared to the squared velocity envelopes of data traces (solid blue lines) from (a) Papua New Guinea data and (b) Eastern China-Russia border region.

744
745
746
747
748
749
750
751
752
753
754
755
756
757
758
759
760
761
762
763
764
765
766
767
768
769
770
771
772
773
774
775
776
777
778
779
780
781
782
783
784

	$Q_{ses} \pm \delta Q_{ses}$	$\tau_m \pm \delta \tau_m$ (sec)
MODEL 1	0.004167 ± 0.00028	3.800 ± 0.004
MODEL 2	0.005000 ± 0.00034	3.790 ± 0.004
MODEL 3	0.005747 ± 0.00066	4.600 ± 0.010
MODEL 4	0.007100 ± 0.0005	3.630 ± 0.007
MODEL 5	0.002900 ± 0.0003	1.980 ± 0.005

Table 1 : Apparent attenuation parameters and their errors estimated for the five simulated models using probability density functions shown on Fig. 5..

	Q_{scs}	<i>Scattering Attenuation</i> <i>Apparent Attenuation</i>	<i>Intrinsic Attenuation</i> <i>Apparent Attenuation</i>
MODEL 1 (PREM)	240		100 %
MODEL 2 (Tomographic dVs/Vs model (exponential ACF, a = 10km) + PREM)	200	16.7 %	83.3 %
MODEL 3 (Thermodynamic dVs/Vs model for UM only (exponential ACF, a= 10 km) + PREM)	174	27.5%	72.5%
MODEL4 (Thermodynamic dVs/Vs model for both UM and LM (exponential ACF, a = 10 km) + PREM)	140	41.3 %	58.7 %
MODEL 5 (Thermodynamic heterogeneity + no intrinsic attenuation + PREM velocities and densities)	340	100 %	

785
786
787
788
789
790
791

Table 2 : Estimated relative contributions to apparent $1/Q_{scs}$.